

Ablation of insulators under the action of short pulses of X-ray plasma lasers and free-electron lasers

N. A. Inogamov,^{a)} S. I. Anisimov, Yu. V. Petrov, and V. A. Khokhlov

L. D. Landau Institute of Theoretical Physics, Russian Academy of Sciences, Chernogolovka, Moscow Oblast

V. V. Zhakhovskii

Consolidated High-Temperature Institute, Russian Academy of Sciences, Moscow

University of South Florida, Tampa, Florida

A. Ya. Faenov and T. A. Pikuz

Consolidated High-Temperature Institute, Russian Academy of Sciences, Moscow

Kansai Institute of Optical Research, Japan Atomic Energy Agency, Kyoto, Japan

V. E. Fortov and I. Yu. Skobelev

Consolidated High-Temperature Institute, Russian Academy of Sciences, Moscow

Y. Kato

Higher Education in the Creation of New Branches of the Optics Industry, Hamamatsu, Shizuoka, Japan

V. V. Shepelev

Institute of Design Automation, Russian Academy of Sciences, Moscow

Y. Fukuda, M. Tanaka, M. Ishino, M. Nishikino, M. Kando, and T. Kawachi

Kansai Institute of Optical Research, Japan Atomic Energy Agency, Kyoto, Japan

M. Kishimoto

University of South Florida, Tampa, Florida

M. Nagasono, K. Tano, and T. Ishikawa

XFEL RIKEN SPring-8, Hyogo, Japan

N. Ohashi, M. Yabashi, and T. Togashi

XFEL RIKEN SPring-8, Hyogo, Japan

Japanese Research Institute of Synchrotron Radiation, SPring-8, Hyogo, Japan

Y. Senda

Japanese Research Institute of Synchrotron Radiation, SPring-8, Hyogo, Japan

(Submitted January 28, 2011)

Opticheskiĭ Zhurnal **78**, 5–15 (August 2011)

An experimental and theoretical study has been carried out of the ablation of a solid insulator with a wide band gap (LiF) under the action of ultrashort laser pulses of the UV range, obtained in a free-electron laser (pulse width $\tau_L = 0.3$ ps, photon energy $\hbar\omega_L = 20.2$ eV), and the soft X-ray region, obtained in a silver-plasma laser ($\tau_L = 7$ ps, $\hbar\omega_L = 89.3$ eV). A comparison is made of the results obtained on the two laser systems. It is shown that the ablation threshold is about the same for both lasers. A theory is presented that explains the weak growth of the ablation mass with increasing surface energy density of the laser radiation (the fluence) in the case of X-ray lasers as a result of the transition from spallation close to the ablation threshold to evaporative ablation at high fluence values. © 2011 Optical Society of America.

INTRODUCTION

The ablation of solids under the action of short pulses of laser radiation in the optical or soft-X-ray region has great significance from both a theoretical and a practical viewpoint. It is used for microstructural processing of the surfaces of metals, semiconductors, and insulators. This article presents the results of experiments and their theoretical investigation for cases in which ultrashort UV and X-ray laser pulses act on solids with various electron-band structures. Experiments carried out on two types of lasers – a silver-plasma X-ray laser (XRL) and an extreme-UV free-electron laser (EUV-FEL), distinguished by the pulse width τ_L and energy $h\omega_L$ of the emitted photons – show a low fluence threshold, characteristic of both, for the start of the ablation. The low ablation threshold means that ultrashort X-ray pulses have higher efficiency by comparison with the longer nanosecond X-ray pulses, as well as by comparison with laser pulses of the optical region—both nanosecond and femtosecond ones. For both of the lasers under consideration in the soft X-ray region, the pulse width τ_L is less than or of the order of the acoustic time $t_s = D_{\text{att}}/c_s$ in which sound with velocity c_s passes through the depth D_{att} to which light penetrates into the sample. In this sense, such short pulses can be called supersonic. They create thermomechanical stresses, which cause spallation. The thermomechanical stresses and the resulting negative pressures determine the character of the ablation at relatively low fluences close to the ablation threshold, when, with moderate heating, the target substance remains in the condensed state and the tensile strength of the bonds of the atoms of the substance becomes important. At higher fluence, the absorption of the radiation of the X-ray laser transforms a heated surface layer of the target to the vapor state, for which such bonds can be neglected.

The laser pulse is absorbed by the electron subsystem of the condensed substance. The energy-exchange rate E_{ei} between the electrons and the ions is limited because of the large difference of their masses. For short laser pulses, the energy-exchange time t_{eq} between the electrons and ions exceeds the pulse width τ_L . This produces a two-temperature situation, in which initially $T_e \gg T_i$, and the temperatures of the electrons and ions equalize in a time of the order t_{eq} : $T_e = T_i$. The fluences that we considered are such that the heating of the target's surface layer of thickness D_{att} corresponds to its thermodynamic state between the triple point and the critical point. The density of the substance during heating differs little from the density of the solid target, while the embedded internal energy arriving at the atom ranges from tenths of an eV to several eV. This is the state of warm dense matter (the WDM region). The ultrashort laser pulses of the optical and X-ray ranges at the initial stage transform the target substance into the two-temperature WDM state, and a hot single-temperature substance is formed only after a delay time of about t_{eq} . The two-temperature stage is an important part of the entire process of ablation of condensed matter under the action of ultrashort laser pulses.

EXPERIMENTS ON X-RAY LASERS

The first experiments on the ablation of insulators by short X-ray laser pulses were carried out at the Kansai Institute of

Optical Research of the Japan Atomic Energy Agency. The X-ray laser available there, based on silver plasma (Ag-XRL) and having a working wavelength of $\lambda = 13.9$ nm, was substantially reconstructed by comparison with our preceding research.^{1,2} In the new experiments, the soft X-rays of a laser based on the transitions of Ni-like Ag ions generated by the first plasma target was amplified as it passed through the plasma of a second silver target.^{3,4} This made it possible to generate a totally coherent beam of X-ray laser radiation. The laser pulse had a mean energy of 300 nJ and a pulse width of $\tau_L = 7$ ps. The Ag-XRL laser operated in the 0.1-Hz regime, with horizontal and vertical angular divergences, respectively, of 1.2 and 0.4 mrad.

The laser beam was focused on a LiF crystal 2 mm thick and 20 mm in diameter, using a spherical Mo/Si multilayer mirror with radius of curvature 1050 mm. The mirror was placed 2715 mm from the exit aperture of the laser at an angle of incidence of 2° . The LiF crystal could be displaced along the beam direction in order to change the focusing conditions on the surface. After each shot, the crystal was displaced perpendicular to the beam to provide a clean target surface for the next shot. A zirconium filter 0.2 μm thick was placed in front of the mirror 800 mm from the laser's exit aperture in order to suppress the optical radiation and X-rays from the plasma created by the picosecond optical laser. The transmittance of the zirconium filter and the reflectance of the Mo/Si mirror at a wavelength of $\lambda = 13.9$ nm were, respectively, 49% and 50%, and this provided an energy of about 75 nJ in each shot on the surface of the LiF crystal.

Experiments with the free-electron laser were carried out on the SPring-8 compact SASE source (SCSS). This apparatus can generate laser pulses in the hard-UV region.^{5–7} In our experiments, the wavelength was 61.5 nm. We used the single-pulse regime, which makes it possible to measure the laser energy at each shot.⁷ The energy of one SCSS pulse varied from 4 to 11 μJ , with a pulse width of about 300 fs.⁶

We used a Kirkpatrick–Baez microscope having ellipsoidal and cylindrical mirrors with a multilayer SiC coating for focusing a beam of hard-UV radiation at about 100 cm from the mirrors. The transmittance of the microscope is about 70%. The LiF crystal could be displaced both along and across the direction of the laser beam, as in the case of experiments on the Ag-XRL. To find the threshold fluence for starting to ablate the LiF, we varied the beam energy and its focusing on the surface of the crystal, diverging from the position of best focusing by up to 40 mm.

To determine the shape of the focal spot in the cases of the Ag-XRL and SCSS lasers, we used the luminescence of the stable color centers (F centers) formed in the LiF crystal after the laser pulses act on it.^{8–11} This allows us to find the actual value of the fluence on the target surface and to more accurately estimate the threshold fluence for ablation. The luminescence of the F centers was observed by means of a confocal Olympus fluorescence laser microscope (model FV300). An Ar laser (488 nm) was used in the microscope to excite F centers with luminescence in the 500–800-nm range, with peaks at 530 nm for F_2 centers and 670 nm for F_3+ centers. To observe surface breakdown of the crystal, we used an Olympus BX60 microscope in the

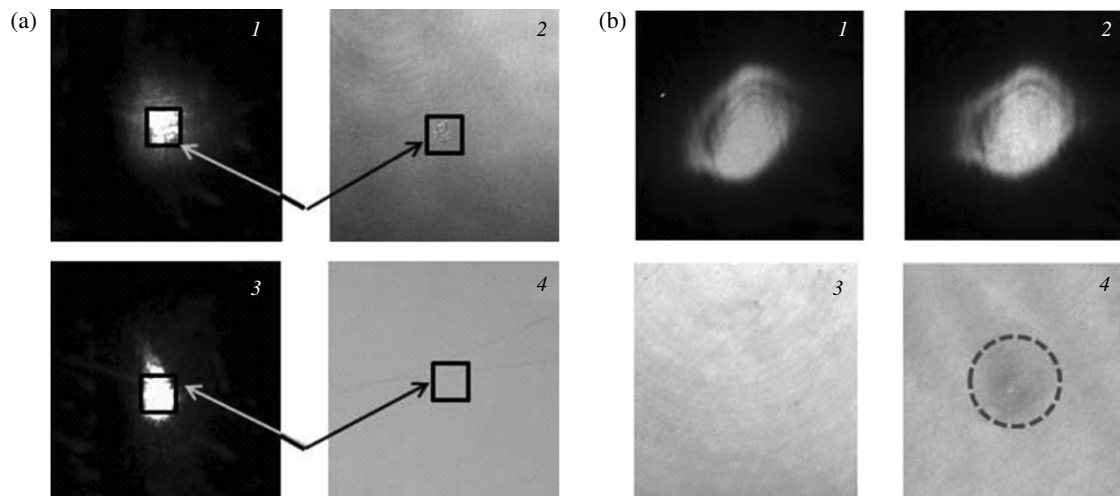


FIG. 1. (a) 1—Luminescence image of the irradiation region of a LiF crystal by an XRL at the transitions of Ni-like Ag ions with energy density $I = 10.8 \text{ mJ/cm}^2$ in the focal plane ($\Delta f = 0 \text{ mm}$), 2—visible image of the same part of the surface of the LiF crystal. The squares outline the zone on which ablation occurred. 3 and 4—Luminescence and visible images of the irradiation region of a LiF crystal by an XRL with energy density $I = 5.3 \text{ mJ/cm}^2$ in a plane distant from the focus by $\Delta f = 1 \text{ mm}$. The squares show that no ablation is observed in the irradiation zone. (b) 1 and 3—Luminescence and visible images of the irradiation region of a LiF crystal by a free-electron laser (FEL) beam at flux density $I = 7.1 \text{ mJ/cm}^2$. There is no ablation. 2 and 4—Luminescence and visible images of the irradiation region of a LiF crystal by an FEL-laser beam at flux density $I = 9.2 \text{ mJ/cm}^2$. The dashed circle on image 4 outlines the ablation region (0.035 mm^2).

visual and differential modes. Using the Topometrix Explorer atomic-force microscope, we measured the transverse cross section of the ablation craters. Typical images of the irradiation region of the LiF crystal by the Ag-XRL and SCSS lasers for various positions of the focal point are shown in Figs. 1(a) and 1(b).

We performed two series of experimental studies to determine the ablation threshold of the LiF crystal under the action of the short-pulse-width radiation of the X-ray lasers. In the first series of experiments, carried out on the Ag-XRL, we repeated our previous studies^{1,2} of LiF ablation under the action of a 7-ps laser pulse, but this time we used a second silver target to obtain a more coherent radiation beam with repetition rate 0.1 Hz.^{12,13} Even though the total energy in the laser was lower in the new experiments than in the previous ones, we obtained a more stable ablation pattern on the LiF because of the better quality of the focusing mirror. To measure the ablation threshold of lithium fluoride, we varied the position of the focus spot relative to the target in order to reduce the beam intensity on its surface. As can be seen from Fig. 1(a), the new results confirm the results obtained in our previous experiments—in particular, the relatively low value of the ablation threshold of LiF under the action of the picosecond Ag-XRL ($F_{\text{abl}} \approx 10 \text{ mJ/cm}^2$). This value is significantly lower than the ablation thresholds under the action of nanosecond X-ray or optical lasers, as well as that of ultrashort femtosecond lasers.

The second series of experiments was carried out on the SCSS free-electron laser. This makes it possible to measure the beam energy in each shot and to study the damage of the lithium fluoride crystal over a larger area and in a wider fluence range. This is an important advantage of the SCSS apparatus by comparison with the Ag-XRL described above. As can be seen from Figs. 1(b), 2, 3, surface damage of the LiF crystal under the action of the SCSS-laser radiation was observed not only when the focal spot of the beam was on the target

surface, but also when it was 26 mm away from the surface. This made the ablation zone reach the very great value of about 0.35 mm^2 . The possibility of strongly defocusing the laser beam and varying its intensity made it possible to strongly vary the fluence on the target surface and to measure the threshold fluence for ablation of the LiF with good accuracy. It can be seen from Fig. 1(b) that a fluence of about 7.1 mJ/cm^2 is still not enough to begin ablation under the action of a beam of hard-UV radiation from the SCSS apparatus. However, even at a fluence of about 9.2 mJ/cm^2 , an ablation spot can be distinctly seen on the surface of the crystal.

It is interesting to compare the depths of the ablation craters when lithium fluoride has been irradiated by a UV laser with different values of fluence. We found that the smallest crater depth that appears when there is significant fluence close to the ablation threshold is 10–15 nm (Fig. 2). At the same time, increasing the fluence to 80 mJ/cm^2 does not substantially increase the ablation depth, which amounts to 30–35 nm for such fluence. This result is significantly different from the results of irradiating the LiF surface with the 7-ps pulse of the Ag-XRL laser, when we already observed an ablation crater 40–50 nm deep close to the ablation threshold. Figure 3 shows the results of a depth measurement of the ablation crater for fluences of UV radiation that exceed 80 mJ/cm^2 . They again show that the ablation depth of the UV laser weakly depends on the fluence. As follows from Fig. 3, with fluences of 110–150 mJ/cm^2 , the ablation depth remains small and is about 30–40 nm.

PHYSICAL MODEL OF THE INTERACTION OF AN ULTRASHORT PULSE OF AN X-RAY LASER WITH AN INSULATOR

The system of equations that describes the variation of the state of a dielectric target and its motion when it interacts with an ultrashort laser pulse in the soft X-ray region can be written

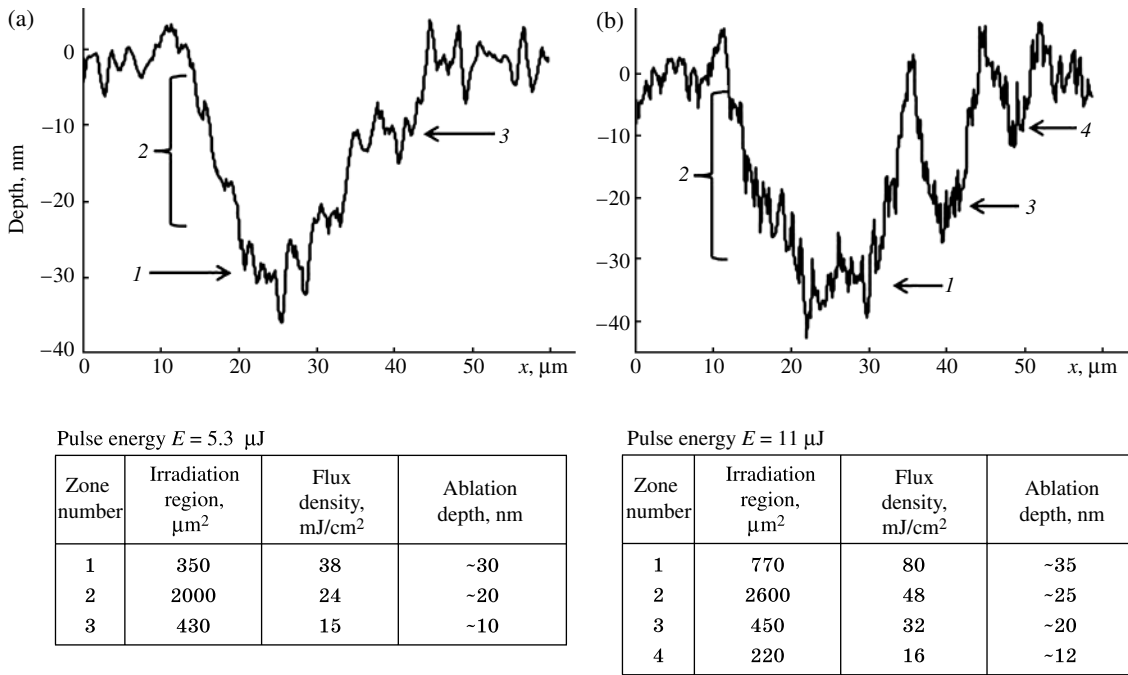


FIG. 2. Density patterns from images obtained by atomic microscope, for sections of a LiF crystal irradiated by a pulsed FEL in a plane distant from the plane of best focus by 5 mm.

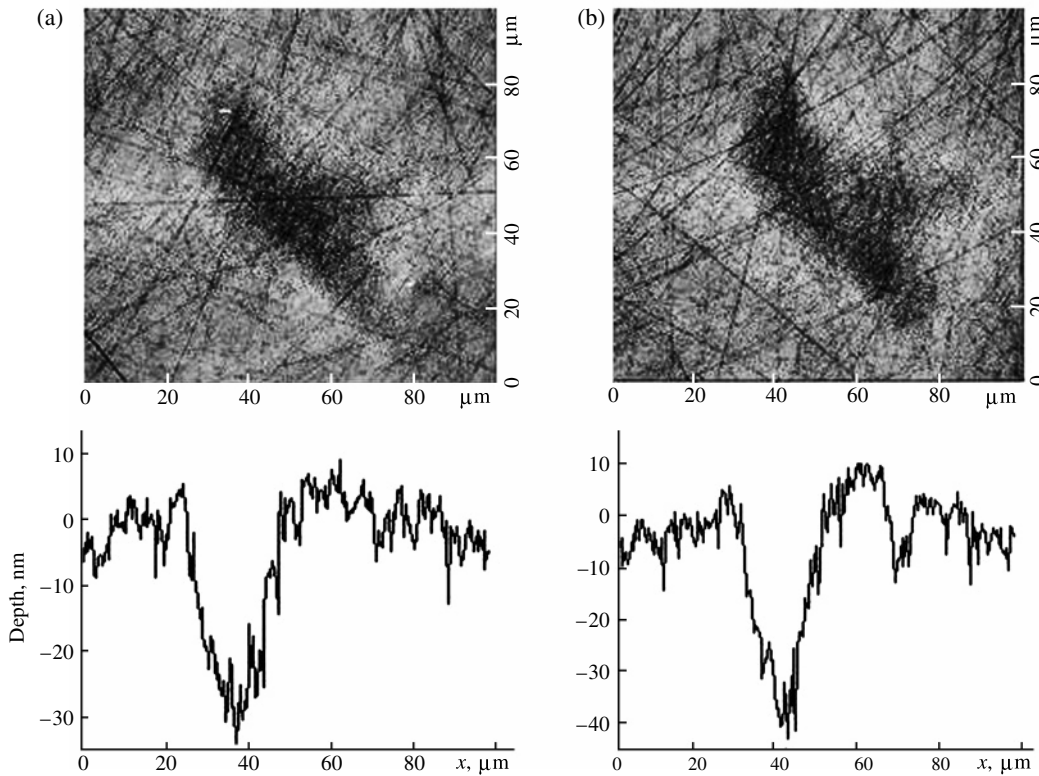


FIG. 3. Surface-irradiation zones of a LiF crystal after one burst of an FEL, obtained by atomic microscope, and density patterns of the surface profile: (a) energy $E = 6.35 \mu\text{J}$ (energy density $I = 110 \text{ mJ}/\text{cm}^2$), ablation depth about 35 nm; (b) energy $E = 10.3 \mu\text{J}$ (energy density $I = 150 \text{ mJ}/\text{cm}^2$), ablation depth about 40 nm. The density patterns show a slow increase of the ablation depth with increasing energy density of the incident radiation.

in the form

$$n_p \frac{\partial Z}{\partial t} = \frac{I}{\hbar \omega_L D_{\text{att}}} + v_{\text{imp}} n_e - k_{\text{rec}} n_e^3, \quad (1)$$

$$\rho^0 \frac{\partial (E_e / \rho)}{\partial t} = \frac{\rho^0 I}{\rho D_{\text{att}}} - n_p^0 \Delta \frac{\partial Z}{\partial t} - \frac{\rho^0}{\rho} \alpha (T_e - T_i) - p_e \frac{\partial u}{\partial x^0}, \quad (2)$$

$$\rho^0 \frac{\partial(E_i/\rho)}{\partial t} = \frac{\rho^0}{\rho} \alpha (T_e - T_i) - p_i \frac{\partial u}{\partial x^0}, \quad (3)$$

$$\rho^0 \frac{\partial u}{\partial t} = -\frac{\partial p}{\partial x^0}, \quad (4)$$

$$\rho(x^0, t) \frac{\partial x(x^0, t)}{\partial t} = \rho^0, \quad (5)$$

$$\frac{\partial x(x^0, t)}{\partial t} = u(x^0, t). \quad (6)$$

Equation (1) describes the population variation $Z = n_e/n_p$ of the conduction band by electrons (the degree of ionization), while Eqs. (2) and (3) describe the variation of the internal energy of the electrons and ions, respectively. Equations (1)–(3) are solved in combination with the one-dimensional Lagrangian hydrodynamic Eqs. (4)–(6). Lagrangian variable x^0 , associated with a moving substance, is the initial position of a material particle. Direction x is perpendicular to the surface being irradiated. The one-dimensional approximation is valid, since the transverse dimensions of the focal spot are much greater than the penetration depth of the light, $D_{\text{att}} = 9$ nm (Ref. 14) when the photon energy is 20.2 eV. Equation (1), which describes the transition of the electrons from the valence band to the conduction band, is missing from the system of equations that we used earlier in discussing the ablation of metals under the action of ultrashort laser pulses in the optical region.¹⁵ It gives the variation of the electron concentration in the conduction band in a moving material particle with Lagrangian variable x^0 due to photoionization, impact ionization, and collisional recombination. The contributions of photorecombination and ambipolar diffusion are small on our time interval and can be neglected in Eq. (1), as can the electron and ionic thermal conductivities in Eqs. (2) and (3). The laser-energy flux density I [W/cm²] gives in Eq. (1) the energy release per unit volume of $\partial I/\partial x = -I/D_{\text{att}}$ and laser pumping of the electrons into the conduction band when an electron from the valence band absorbs a photon of energy $\hbar\omega_L$ and has the form

$$I(x^0, t) = \frac{F}{\sqrt{\pi}\tau_L} \exp\left(-\frac{t^2}{\tau_L^2}\right) \exp\left(-\frac{x^0}{D_{\text{att}}}\right). \quad (7)$$

Here F [mJ/cm²] is the fluence (the surface energy density) absorbed by the insulator. The thickness of the LiF disk is 2 mm $\gg D_{\text{att}} \approx 9$ nm, and the fluence is completely absorbed in the surface layer, resulting in the exponential dependence of I on x^0 in Eq. (7). The initial position of the insulator corresponds to $x > 0$. The time is counted from the maximum of the laser pulse in Eq. (7). The calculations begin at $t_{\text{start}} = -5\tau_L$.

In Eq. (2), E_e is the energy of the electrons in the conduction band, measured from the bottom of the band. It includes the zeroth Fermi energy of electrons with concentration n_e and the temperature contribution and can be written in the form of the interpolation expression

$$E_e(T_e, \rho, Z) = \frac{1}{2} n_e \sqrt{\left(\frac{6}{5} E_F\right)^2 + (3k_B T_e)^2}. \quad (8)$$

Here $E_F = (3\pi^2)^{2/3} \hbar^2 n_e^{2/3} / 2m_e$ is the Fermi energy.¹⁶ The electron pressure in the conduction band is

$$p_e = (2/3) E_e. \quad (9)$$

The electron pressure p_e and ion pressure p_i in Eqs. (2), (3) determine the work of expansion $p_e \partial u / \partial x^0$ and $p_i \partial u / \partial x^0$ in the electron and ion subsystems. The variation of the pulse in dynamic Eq. (4) is determined by the gradient of the total pressure $p = p_e + p_i$.

THE EQUATION OF STATE AND THE KINETIC COEFFICIENTS IN TWO-TEMPERATURE LiF

To integrate the system of differential Eqs. (1)–(6), it is necessary to know the equation of state of the target substance, as well as the kinetic coefficients: the impact-ionization frequency ν_{imp} , the three-particle recombination coefficient k_{rec} , and the electron–ion energy-exchange coefficient α . As shown in Ref. 17, at moderate temperatures, identical for ions and electrons, the equation of state of LiF with high accuracy coincides with the equation of state of aluminum. To illustrate this, Fig. 4 shows the cold-compression curves and impact adiabats of these two substances. The fact that these curves coincide makes it possible for the ionic contribution $E_i(T_i, \rho)$ and $p_i(T_i, \rho)$ in LiF to use the ionic contribution to these quantities from the well-known wide-range equation of state of aluminum.^{17,18} The contribution of the conduction electrons to the equation of state is taken into account by the approximating expression given by Eq. (8). The impact-ionization frequency ν_{imp} in Eq. (1) was taken from Ref. 21, as was done in Ref. 2. The three-particle recombination coefficient is found from the principle of detail balance.²¹

In calculating the electron–ion energy-exchange coefficient α , we mainly took into account the strong interaction of the conduction electrons that result from being excited from the valence band by photoionization and impact ionization with the transverse optical phonons of the ionic LiF crystal. Such interaction results in a strong increase of coefficient α as the number of electrons in the conduction band increases ($\alpha \rightarrow 0$ for low concentrations of conduction electrons, and this manifests the difference of the electron–ion energy exchange in an insulator and a metal, including aluminum^{22–26}). When the electron concentrations in the conduction band are significant, part of the bonds in the LiF crystal begin to make a transition from ionic to covalent, and neutral atoms begin to form in the crystal. This reduces coefficient α , with a maximum that exceeds its value for aluminum by a factor of 1.7–2.

The resulting kinetic coefficients were used along with the equation of state of LiF for a numerical solution of the two-temperature system of hydrodynamic Eqs. (1)–(6).

THE HEATING AND EXPANSION DYNAMICS OF THE LiF CRYSTAL

The system of Eqs. (1)–(6) with parameters determined in the two preceding sections was used for numerical modelling of the action of hard-UV radiation from a free-electron laser on the insulating LiF crystal in accordance with the experimental conditions described in the section on X-ray lasers. The formation and propagation of an impact wave in the crystal

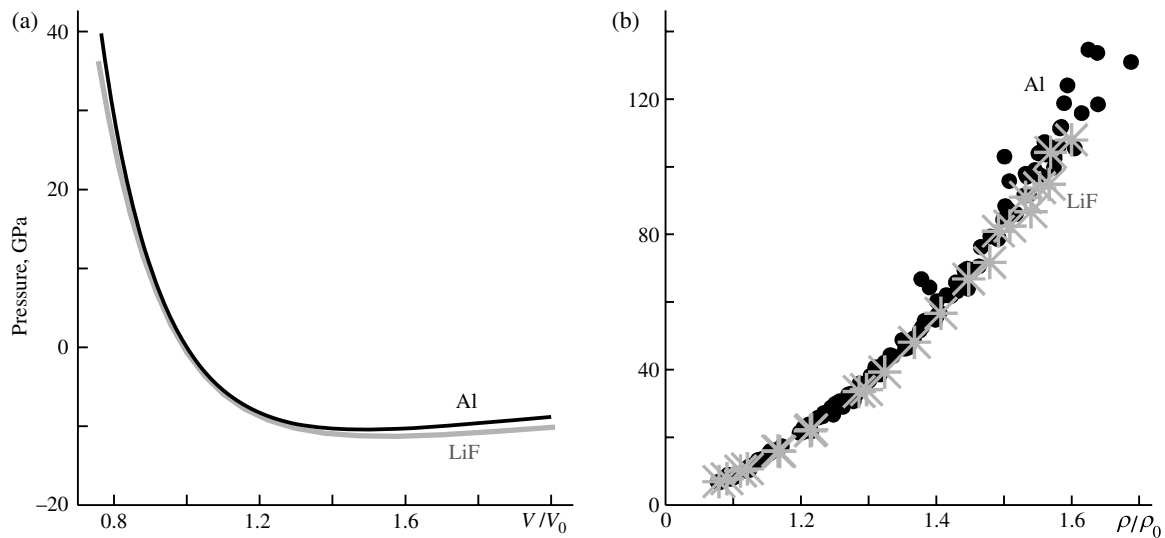


FIG. 4. (a) “Cold curves,” also called the zeroth isotherm $p(\rho, T = 0)$ or the zeroth adiabat $p(\rho, S = 0)$, and (b) the impact adiabats for LiF (Ref. 17) and Al.^{19,20}

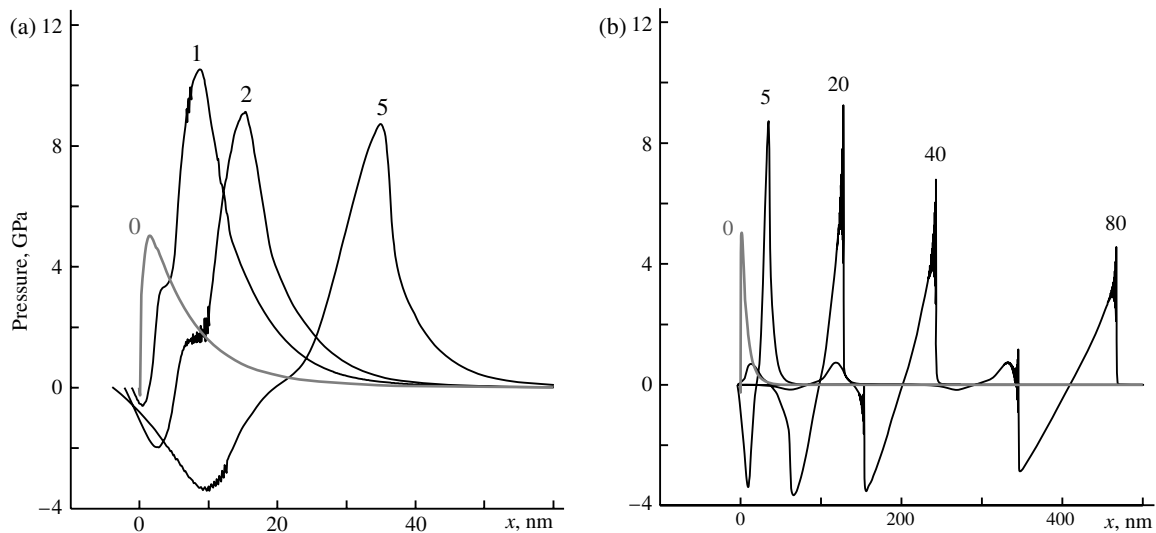


FIG. 5. (a) Formation of a compression wave. (b) Appearance of an impact wave as a result of the breakdown of the compression wave after a pulse from an EUV-FEL laser is delivered with intensity close to the ablation threshold ($\tau_L = 300$ fs, fluence $F = 10$ mJ/cm²). The numbers over the curves denote the time in picoseconds that have elapsed since the time of the maximum intensity of the laser pulse.

after the action of a laser pulse is shown in Figs. 5 and 6, with the parameters that characterize the experiment: pulse width $\tau_L = 300$ fs, photon energy 20.2 eV, and penetration depth $D_{\text{att}} = 9$ nm. The heating depth D_{att} is less than in the case of metals.^{15,20,27,28} At the same time, the skin-layer thickness in metals at optical frequencies is comparable with D_{att} , and they exhibit rapid supersonic propagation of an electronic thermal wave, which is absent in insulators. Therefore, an impact wave appears in LiF earlier than in metals.

Half the energy of the laser pulse has been liberated at time $t = 0$; see Eq. (7). The total pressure $p = p_i + p_e$ reaches its maximum somewhat later than the end of the action of the pulse. First, this is because the electron–ion energy-exchange time is greater than $\tau_L = 300$ fs; second, it is because the pressure increases as energy is transported from the electrons to the ions, since the Grüneisen coefficient of the ions is greater than that of the electrons (pressure p_e is less than p_i

when the internal energy of the electrons and ions is equal). Passing through some distance into the depth of the sample, the resulting compression wave breaks up as a consequence of its nonlinearity and forms a pressure discontinuity (an impact wave). The greater the nonlinearity that characterizes the compression wave (the greater the fluence F and the accordingly the pressure p), the faster it breaks up. The impact wave thus formed attenuates as it propagates along the sample (Fig. 6). The impact wave attenuates faster for strongly nonlinear waves.

Near the ablation threshold $F_{\text{abl}} \approx 10$ mJ/cm², the maximum electron temperature is $T_e \approx 20$ kK, while the maximum degree of ionization Z is about 3%. Electron–ion relaxation lasts for time $t_{\text{eq}} \sim 1$ ps. The maximum ionic temperature T_i equals 1.5 kK. At a fluence of $F = 180$ mJ/cm² (the largest in the experiments), the corresponding parameters are as follows: $T_{e|\text{max}} \approx 110$ kK, $Z_{|\text{max}} \approx 0.4\text{--}0.5$, and

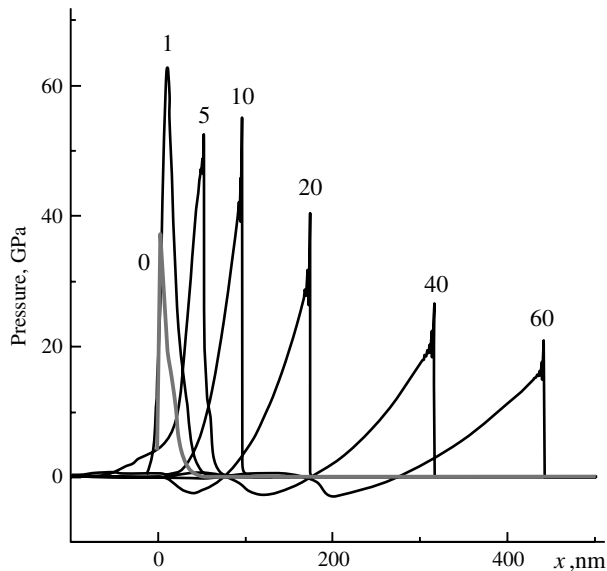


FIG. 6. Formation of a powerful acoustic perturbation and an impact wave after a strong pulse is delivered from an EUV-FEL laser ($\tau_L = 300$ fs, $F = 180$ mJ/cm²). The numbers over the curves denote the time in picoseconds that have elapsed since the time of the maximum intensity of the laser pulse.

$T_{i|\max} \approx 10$ kK (at a time close to the instant at which electron–ion equilibrium is established $t_{eq} \sim 1$ ps). Short UV laser pulses with low fluence values $F \sim F_{abl}$ and those with large values $F \sim 200$ mJ/cm² create negative pressures that differ in magnitude, causing spallation. The mechanism of spallation of insulators under the action of ultrashort pulses of XRLs was proposed in Ref. 2, where we experimentally and theoretically discussed only the region of fluences of the Ag-XRL laser close to the threshold value. Here, for the SCSS laser, we shall consider ablation in a wide range of fluences.

It can be seen from Figs. 5–7 that, in the near-threshold case, negative pressures are reached at an early stage at a small depth of ≈ 10 nm, and their amplitude $|p_{neg}| \approx 3.5$ GPa is about half the amplitude of the compressive wave. At high fluences, the negative pressures appear later, at a significant depth, with their maximum amplitude $|p_{neg}|_{\max}$ being of the same order of magnitude as in the near-threshold case. However, it now constitutes only a small part (less than 0.1 when $F = 180$ mJ/cm²) of the maximum pressure on the compression wave.

The $|p_{neg}|_{\max}(x^0)$ dependences in Fig. 7 show how the maximum tensile stresses $|p_{neg}|_{\max}$ vary in space and in time when the compression and expansion waves propagate into the depth of the LiF crystal. As was said earlier, we used the equation of state of aluminum^{17–19} when numerically modelling the LiF-ablation dynamics. For aluminum, the maximum modulus of the negative pressure of the cold substance is $|p_{neg}|_{\max}(T = 0) \approx 12$ GPa (according to Ref. 20 and the literature references indicated in it). Neglecting the nucleation kinetics in the metastable region, fragmentation appears when the state of the target substance on the phase plane is at a point that lies on the spinodal. Our calculations show that, in the cases shown in Figs. 5–7, in the cold part of the target, tensile stresses close to $|p_{neg}|_{\max}(T = 0)$ for aluminum are not attainable at the fluence values that are used. Consequently, we cannot observe breakaway of a cold

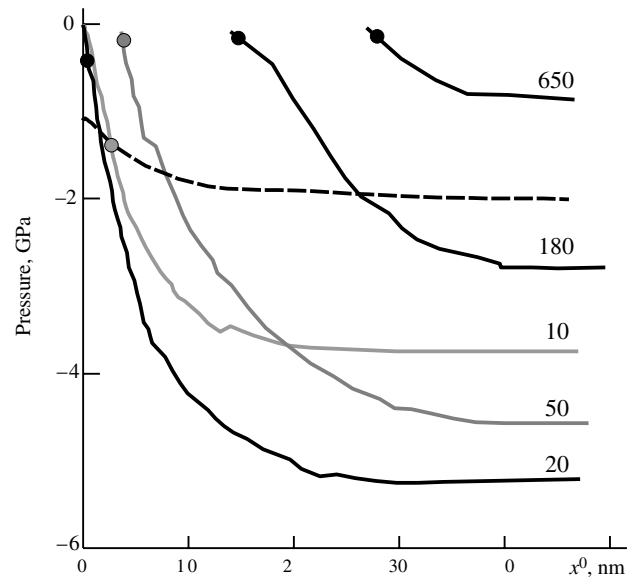


FIG. 7. Maximum tensile stress $|p_{neg}|_{\max}$ vs Lagrange coordinate x^0 (solid curves). The numbers on the curves indicate the fluence F in mJ/cm². The dashed curve is the strength p_{lim} of the material for the case $F = 10$ mJ/cm².

spallation plate from the rest of the target, as occurred in Ref. 20, but we observe evaporation and fragmentation of the hot substance in a thin surface layer at large values of fluence. This means that the state of the target substance on the phase plane in our calculations is at a point lying on the high-temperature part of the spinodal (not far from the critical point) and cannot reach the cold part of the spinodal, corresponding to the value $|p_{neg}|_{\max}(T = 0)$.

We estimated the thickness of the cold spallation plate as follows: First of all, the temperature dependence of the strength of the target substance $p_{lim}(T)$ was determined. The value of $p_{lim}(T)$ was taken at the level of 30–60% of the strength of aluminum, known at high deformation rates from the data of Ref. 27, and can be approximated by the expression $p_{lim}(T)[\text{GPa}] = -2.2 + 0.7T[\text{kK}]$. The $T(x)$ dependence obtained in the modelling now makes it possible to obtain the $p_{lim}(T(x^0)) = p_{lim}(x^0)$ dependence. The dashed curve in Fig. 7 shows the strength profile $p_{lim}(x^0)$ of the target substance when it is heated with a pulsed UV laser as a function of the Lagrangian coordinate of a material point of the target. The intersection of the $p_{lim}(x^0)$ and $|p_{neg}|_{\max}(x^0)$ curves gives the value of the Lagrangian coordinate of the rupture point. The intersection point of the $p_{lim}(x^0)$ and $|p_{neg}|_{\max}(x^0)$ curves at a fluence of $F = 10$ mJ/cm² is shown by a circle in Fig. 7. Similar circles show the points where these curves intersect for other fluences.

ACKNOWLEDGMENTS

This work was supported by the Japanese Ministry of Education, Science, Sport, and Culture (Grant-in-Aid for Kiban A No. 20244065, Kiban B No. 21360364), the Russian Foundation for Basic Research (Projects 10-02-00434-a, 09-02-92482-MNKS-a, 10-02-00345), and Fundamental Research Programs Nos. 2 and 21 of the Presidium of the Russian Academy of Sciences.

- ¹A. Ya. Faenov, N. A. Inogamov, V. V. Zhakhovskii, V. A. Khokhlov, K. Nishihara, Y. Kato, M. Tanaka, T. A. Pikuz, M. Kishimoto, M. Ishino, M. Nishikino, T. Nakamura, Y. Fukuda, S. V. Bulanov, and T. Kawachi, "Low-threshold ablation of dielectrics irradiated by picosecond soft X-ray laser pulses," *Appl. Phys. Lett.* **94**, 231107 (2009).
- ²N. A. Inogamov, A. Ya. Faenov, V. A. Khokhlov, V. V. Zhakhovskii, Yu. V. Petrov, I. Yu. Skobelev, K. Nishihara, Y. Kato, M. Tanaka, T. Pikuz, M. Kishimoto, M. Ishino, M. Nishikino, Y. Fukuda, S. V. Bulanov, T. Kawachi, S. I. Anisimov, and V. E. Fortov, "Spallative ablation of metals and dielectrics," *Plasma Phys.* **49**, 455 (2009).
- ³M. Nishikino, N. Hasegawa, T. Kawachi, H. Yamatani, K. Sukegawa, and K. Nagashima, "Characterization of a high-brilliance soft X-ray laser at 13.9 nm by use of an oscillator-amplifier configuration," *Appl. Opt.* **47**, 1129 (2008).
- ⁴Y. Ochi, N. Hasegawa, T. Kawachi, and K. Nagashima, "Development of a chirped pulse amplification laser with zigzag slab Nd:glass amplifiers dedicated to X-ray laser research," *Appl. Opt.* **46**, 1500 (2007).
- ⁵T. Inagaki, S. Imoue, M. Ishi, Y. Kim, H. Kimura, M. Kitamura, T. Kobayashi, H. Maesaka, T. Masuda, S. Matsui, T. Matsushita, X. Marechal, M. Nagasono, H. Ohashi, T. Ohata, T. Ohshima, K. Onoe, K. Shirasawa, T. Takagi, S. Takahashi, M. Takeuchi, K. Tamasaku, R. Tanaka, Y. Tanaka, T. Tanikawa, T. Togashi, S. Wu, A. Yamashita, K. Yanagida, C. Zhang, H. Kitamura, and T. Ishikawa, "A compact free-electron laser for generating coherent radiation in the extreme ultraviolet region," *Nat. Photonics* **2**, 555 (2008).
- ⁶T. Shintake, H. Tanaka, T. Hara, T. Tanaka, K. Togawa, M. Yabashi, Y. Otake, Y. Asano, T. Fukui, T. Hasegawa, A. Higashiyama, N. Hosoda, T. Inagaki, S. Inoue, Y. Kim, M. Kitamura, N. Kumagai, H. Maesaka, S. Matsui, M. Nagasono, T. Ohshima, T. Sakurai, K. Tamasaku, Y. Tanaka, T. Tanikawa, T. Togashi, S. Wu, H. Kitamura, T. Ishikawa, T. Asaka, T. Bizen, S. Goto, T. Hirono, M. Ishii, H. Kimura, T. Kobayashi, T. Masuda, T. Matsushita, X. Marechal, H. Ohashi, T. Ohata, K. Shirasawa, T. Takagi, S. Takahashi, M. Takeuchi, R. Tanaka, A. Yamashita, K. Yanagida, and C. Zhang, "Stable operation of a self-amplified spontaneous-emission free-electron laser in the extremely ultraviolet region," *Phys. Rev. ST Accel. Beams* **12**, 070701 (2009).
- ⁷M. Kato, N. Saito, T. Tanaka, Y. Morishita, H. Kimura, H. Ohashi, M. Nagasono, M. Yabashi, K. Tono, T. Togashi, A. Higashiyama, and T. Ishikawa, "Pulse energy of the extreme-ultraviolet free-electron laser at SPring-8 determined using a cryogenic radiometer," *Nucl. Instrum. Methods Phys. Res. A* **612**, 209 (2009).
- ⁸G. Baldacchini, S. Bollanti, F. Bonfigli, P. Di Lazzaro, A. Ya. Faenov, F. Flora, T. Marolo, R. M. Monteverdi, D. Murra, E. Nichelatti, T. Pikuz, A. Reale, L. Reale, A. Ritucci, and G. Tomassetti, "Point defects in lithium fluoride by EUV and soft X-rays exposure for X-ray microscopy and optical applications," *IEEE J. Sel. Top. Quantum Electron.* **10**, 1435 (2004).
- ⁹G. Baldacchini, S. Bollanti, F. Bonfigli, F. Flora, P. Di Lazzaro, A. Lai, T. Marolo, R. M. Monteverdi, D. Murra, A. Faenov, T. Pikuz, E. Nichelatti, G. Tomassetti, A. Reale, L. Reale, A. Ritucci, T. Limongi, L. Palladino, M. Francucci, S. Martellucci, and G. Petrocelli, "Soft X-ray submicron imaging detector based on point defects in LiF," *Rev. Sci. Instrum.* **76**, 113104 (2005).
- ¹⁰G. Tomassetti, A. Ritucci, A. Reale, L. Palladino, L. Reale, L. Arrizza, G. Baldacchini, F. Bonfigli, F. Flora, L. Mezi, R. M. Monteverdi, S. V. Kukhlevsky, A. Faenov, T. Pikuz, and J. Kaiser, "High-resolution imaging of a soft-X-ray laser beam by color centers excitation in lithium fluoride crystals," *Europhys. Lett.* **63**, 681 (2003).
- ¹¹A. Ya. Faenov, Y. Kato, M. Tanaka, T. A. Pikuz, M. Kishimoto, M. Ishino, M. Nishikino, Y. Fukuda, S. V. Bulanov, and T. Kawachi, "Submicrometer-resolution *in situ* imaging of the focus pattern of a soft X-ray laser by color center formation in LiF crystal," *Opt. Lett.* **34**, 941 (2009).
- ¹²Y. Fukuda, A. Ya. Faenov, T. Pikuz, M. Kando, H. Kotaki, I. Daito, J. Ma, L. M. Chen, T. Homma, K. Kawase, T. Kameshima, T. Kawachi, H. Daido, T. Kimura, T. Tajima, Y. Kato, and S. V. Bulanov, "Soft X-ray source for nanostructure imaging using femtosecond-laser-irradiated clusters," *Appl. Phys. Lett.* **92**, 121110 (2008).
- ¹³Y. Ochi, T. Kawachi, N. Hasegawa, M. Nishikino, T. Ohba, M. Tanaka, M. Kishimoto, T. Kaihori, K. Nagashima, and A. Sugiyama, "Demonstration of submicrojoule, spatially coherent soft-X-ray laser pumped by 0.1 Hz, 10 J, ps laser," *Jpn. J. Appl. Phys.* **48**, 120212 (2009).
- ¹⁴E. D. Palik, ed., *Handbook of Optical Constants of Solids* (Academic Press, New York, 1998).
- ¹⁵N. A. Inogamov, V. V. Zhakhovskii, S. I. Ashtikov, V. A. Khokhlov, Yu. V. Petrov, P. S. Komarov, M. B. Agranat, S. I. Anisimov, and K. Nishihara, "Two-temperature relaxation and melting after absorption of femtosecond laser pulse," *Appl. Surf. Sci.* **255**, 9712 (2009).
- ¹⁶L. D. Landau and E. M. Lifshitz, *Statistical Physics* (Pergamon Press, Oxford, 1980; Nauka, Moscow, 1976).
- ¹⁷<http://teos.ficp.ac.ru/rusbank/>.
- ¹⁸A. V. Bushman, G. I. Kanel, A. L. Ni, and V. E. Fortov, *Intense Dynamic Loading of Condensed Matter* (Taylor & Francis, Washington, 1993).
- ¹⁹J. H. Rose, J. R. Smith, F. Guinea, and J. Ferrante, "Universal features of the equation of state of metals," *Phys. Rev. B* **29**, 2963 (1984).
- ²⁰V. V. Zhakhovskii, N. A. Inogamov, Yu. V. Petrov, S. I. Ashtikov, and K. Nishihara, "Molecular dynamics simulation of femtosecond ablation and spallation with different interatomic potentials," *Appl. Surf. Sci.* **255**, 9592 (2009).
- ²¹I. I. Sobelman, L. A. Vainshtein, and E. A. Yukov, *Excitation of Atoms and Broadening of Spectral Lines* (Springer, 2007).
- ²²Yu. V. Petrov, "Energy exchange between the lattice and electrons in a metal under femtosecond laser irradiation," *Laser Part. Beams* **23**, 283 (2005).
- ²³Z. Lin, L. V. Zhigilei, and V. Celli, "Electron-phonon coupling and electron heat capacity of metals under conditions of strong electron-phonon nonequilibrium," *Phys. Rev. B* **77**, 075133 (2008).
- ²⁴www.faculty.virginia.edu/CompMat/electron-phonon-coupling/.
- ²⁵P. B. Allen, "Theory of thermal relaxation of electrons in metals," *Phys. Rev. Lett.* **59**, 1460 (1987).
- ²⁶X. Y. Wang, D. M. Riffe, Y. S. Lee, and M. C. Downer, "Time-resolved electron-temperature measurement in a highly excited gold target using femtosecond thermionic emission," *Phys. Rev. B* **50**, 8016 (1994).
- ²⁷M. B. Agranat, S. I. Anisimov, S. I. Ashtikov, V. V. Zhakhovskii, N. A. Inogamov, P. S. Komarov, A. V. Ovchinnikov, V. E. Fortov, V. A. Khokhlov, and V. V. Shepelev, "Strength properties of an aluminum melt at extremely high tension rates under the action of femtosecond laser pulses," *Pis'ma Zh. Eksp. Teor. Fiz.* **91**, 517 (2010). [*JETP Lett.* **91**, 471 (2010)].
- ²⁸N. A. Inogamov and Yu. V. Petrov, "Thermal conductivity of metals with hot electrons," *Zh. Eksp. Teor. Fiz.* **137**, 505 (2010). [*JETP* **110**, 446 (2010)].